Interphase Materials by Forced Assembly of Glassy Polymers

R. Y. F. Liu, T. E. Bernal-Lara, A. Hiltner,* and E. Baer

Department of Macromolecular Science and Center for Applied Polymer Research, Case Western Reserve University, Cleveland, Ohio 44106-7202

Received April 20, 2004; Revised Manuscript Received June 16, 2004

ABSTRACT: When two immiscible polymers are brought into intimate contact, highly localized mixing of polymer chains creates an "interphase" region. We have fabricated materials that are entirely interphase by forced assembly of two immiscible polymers. Assemblies of thousands of alternating layers of two polymers, with individual layer thickness on the nanometer size scale of the interphase, were created by layer multiplying coextrusion. The properties of the interphase materials were probed with conventional tools of polymer analysis. In this study, the effect of interaction strength was examined with assemblies that combined an amorphous polyester with a series of styrene−acrylonitrile copolymers that varied in acrylonitrile content from 0 to 30 wt %. Continuous, uniform layers were directly observed using atomic force microscopy. Interphase thickness was extracted from the layer thickness dependence of oxygen permeability. The interphase thickness showed the predicted dependency on the χ parameter and correlated with interphase strength as measured with the T-peel test. Unexpectedly, volumetric properties of the interphase deviated from additive predictions. Correspondence between the decrease in specific volume from macroscopic density and the decrease in free volume hole size from positron annihilation lifetime spectroscopy suggested that densification of the interphase occurred primarily by a decrease in free volume hole size rather than by a decrease in the number of free volume holes. The volume change did not directly correlate with the χ parameter. At present, the origin of the volume change is not clear.

Introduction

The interphase takes on new significance as nanotechnology and microelectronics drive the fabrication of increasingly thin polymer layers. Under these conditions, as bulk polymers become thinner and more interphase-like, departures in physical properties are expected. Changes in segmental mobility as the thickness scale approaches the size scale of the polymer molecule[1,2] will have consequences for the glass transition temperature, thermal stability, adhesion, and transport characteristics.[2−4] Understanding the nanoscale interphase properties is crucial if polymers are to be effectively integrated into modern technologies.

The origin of interfacial mixing is the entropic advantage for chains to diffuse across the boundary. The entropic advantage for crossing the interface is offset by the repulsive interaction energy between immiscible chain segments. It has been recognized for some time that when two polymers are brought into intimate contact, the interface between them is not perfectly sharp. Highly localized mixing of polymer chains creates an "interphase" region. A vast literature attests to the importance of the interphase for polymer adhesion and for compatibility of polymer blends and alloys.[5]

The self-consistent mean-field theory utilized by Helfand and co-workers is the basis of a quantitative relationship between interphase composition and the thermodynamic interaction parameter χ.[6−9] The reduced segment density of polymer A across a symmetric interphase between immiscible polymers A and B of infinite molecular weight is expressed as

$$\frac{\rho_A(x)}{\rho_0} = \frac{1}{1+\xi^2} \tag{1}$$

with

$$\xi \equiv \exp\left[\frac{(6\chi)^{1/2}x}{b}\right] \tag{2}$$

where the reference density is given as $\rho_0(x) = \rho_A(x) + \rho_B(x)$, χ is the interaction parameter, b is the statistical segment step length, and x is the distance from the center of the interphase. It is convenient to define an interphase thickness d_I as

$$d_I = \left|\rho_0\left[\frac{d\rho_A}{dx}\bigg|_{x=0}\right]^{-1}\right| \tag{3}$$

From eq 1 d_I is given as

$$d_I = \frac{2b}{(6\chi)^{0.5}} \tag{4}$$

The composition profile with b taken as 6.0 Å is plotted in Figure 1 as a function of x/d_I. The line tangent to the density profile at $x/d_I = 0$ defines d_I according to eq 3. With its finite dimension, it is reasonable to consider the interphase of an immiscible polymer blend as a third phase with its own characteristic properties.[10]

Experimental determination of interphase properties has challenged the field due to the extremely small volume fraction of interphase in a typical polymer blend. Even measurement of the interphase dimension is difficult and requires extreme care. Nevertheless, existing theoretical and experimental results agree that the dimension of the interphase for immiscible polymers could range from a few to tens of nanometers.[8,11,12] Other physical properties of the interphase, such as density, free volume, and permeability, have been virtually inaccessible.

Fabrication of one-dimensional "polymer blends" by forced assembly of two polymers into many alternating

* Corresponding author: e-mail pah6@case.edu.

10.1021/ma049233r CCC: $27.50
Published on Web 08/05/2004

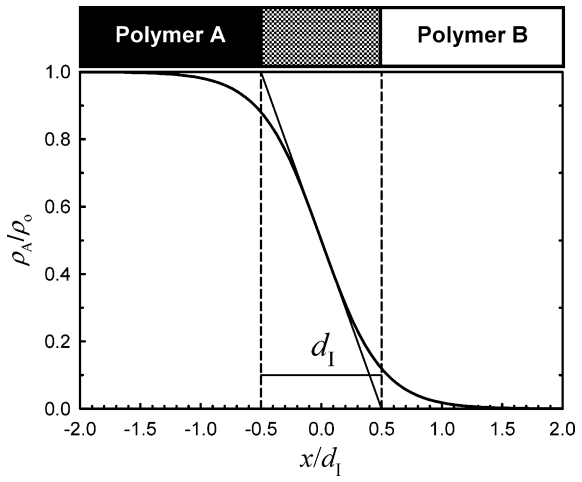

Figure 1. Reduced segment density profile of polymer A across the A−B boundary according to eq 1. The interphase with thickness d_I is taken as a third phase with its own characteristics.

thin layers provides a rich source of models for conventional polymer blends.[13] The process of layer multiplication exploits the viscoelastic nature of polymer melts to repeatedly split, spread, and recombine the coextruded melt stream as shown in Figure 2. The figure illustrates how two elements multiply the number of layers from 2 to 8. An assembly of n die elements produces film or sheet with $2^{(n+1)}$ layers. Typically, the number of layers is in the hundreds, and the layer thickness is on the micron scale, which is comparable to the domain size of conventional polymer blends. Numerous studies illustrate the application of microlayers in elucidating the cooperative microdeformation and crack propagation mechanisms that underlie toughness enhancement of polymer blends[14,15] and in quantifying the role of interfacial adhesion in blend performance.[16−21]

The high specific interface area of microlayers has been exploited to study interfacial phenomena related to miscible polymers.[22−24] The stringent flow conditions of microlayer coextrusion provide a rare opportunity to combine miscible polymers on a small scale with little or no mixing. Raising the temperature begins the interdiffusion process and, in the time frame of the experiment, produces a concentration gradient on the micron size scale of the layer thickness. The gradient is magnified by the number of interfaces and is readily measured experimentally. Unfortunately, the amount of interface in microlayers is not large enough for conventional experimental methods to detect the interphase that is produced by segmental mixing of immiscible polymers. The microlayer thickness is orders of magnitude larger than the dimension of the interphase. Even thinner nanolayers are required.

A recent breakthrough in layer-multiplying coextrusion enables us to decrease the layer thickness by almost 2 orders of magnitude from the microscale to the nanoscale.[25] Nanolayered films consisting of thousands of continuous layers of two polymers with individual layer thicknesses less than 10 nm can be fabricated. The layer thickness can now be made comparable to the interphase dimension. The properties of the interphase that forms during the coextrusion process are multiplied thousands-fold by the number of identical interphases in the assembly. This enables us to use conventional methods of polymer analysis to probe size-scale-dependent properties as nanolayers become thinner and more interphase-like.

An initial study describes the effects of layer thickness on assemblies of two immiscible glassy polymers: polycarbonate (PC) and poly(methyl methacrylate) (PMMA).[25] In conventional DSC thermograms, the two glass transition inflections of the constituent polymers shift closer together as layer thickness decreases below 100 nm, and they merge into a single inflection when the layer thickness is 10 nm or less. This result demonstrates that as the layer thickness becomes comparable to the interphase dimension, the layers lose their integrity as constituent layers, and the film becomes essentially totally interphase.

Gas transport, like the glass transition, probes at the molecular scale and is amenable to interpretation based on free volume concepts.[26−29] Unlike T_g measurements, which require heating the glassy film into the rubbery region where molecular mobility can alter the nanolayer structure, gas transport measurements are performed at ambient temperature and only require that the constituents differ in their gas permeability. If the layers are thick enough to retain their individual properties, permeability is determined primarily by the less permeable constituent of the assembly according to the series prediction. This changes as the layers become thinner and more interphase-like. In the PC/PMMA example, oxygen permeability increases markedly as the layer thickness decreases from 100 to 10 nm.[25]

To further study the interphase of real polymers using forced assembly of nanolayers, we chose to combine a glassy copolyester (PETG) with a series of poly(styrene-*co*-acrylonitrile) copolymers (SAN) of varying acrylonitrile content. We used oxygen permeability to determine the interphase thickness of polymer pairs of varying χ parameter and compared the results with theoretical predictions of eq 4. We also measured interphase strength and tested the results against published models. Furthermore, we characterized the interphase in terms of density and free volume.

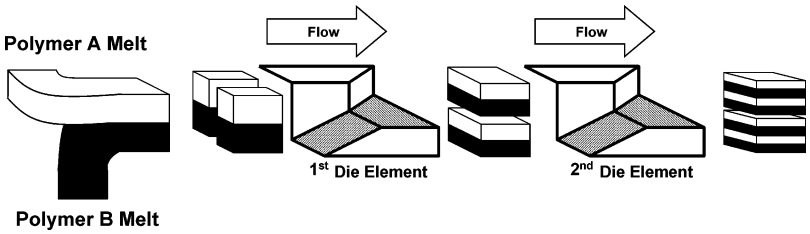

Figure 2. Schematic of layer-multiplying coextrusion used for forced assembly of polymer nanolayers. The figure illustrates how two die elements multiply the number of layers from 2 to 8. An assembly of n die elements produces an assembly with $2^{(n+1)}$ layers.

Table 1. Physical Properties of Polymer Glasses[a]

polymer	δ ($J^{0.5}$ $cm^{-1.5}$)	ρ (g cm^{-3})	T_g (° C)	P	r (Å)	M_w (kg mol^{-1})	PDI	FFV
PETG	19.70	1.2796	82	0.750	2.52	87		0.027
PS	18.41[b]	1.0450	102	14.5	2.85	527	1.7	0.039
SAN17	19.36[b]	1.0700	103	5.54	2.76	159	1.4	0.035
SAN25	20.01[b]	1.0800	107	3.36	2.73	269	1.9	0.034
SAN30	20.26[b]	1.0856	108	2.63	2.72	286	1.8	0.034

[a] δ, solubility parameter; ρ, density; T_g, glass transition temperature; P, permeability in cm^3 (STP) cm m^{-2} day^{-1} atm^{-1}; r, free volume hole radius; M_w, molecular wieght; PDI, polydispersity index; FFV, fractional free volume. [b] From ref 34.

Materials and Methods

An amorphous polyester, poly(ethylene terephthalate-*co*-1,4-cyclohexanedimethylene terephthalate) (PETG), was provided by Eastman Chemical Co. (Eastar 6763) in the form of extruded pellets. This polyester has properties similar to amorphous poly(ethylene terephthalate) (PET), except that PETG does not crystallize readily upon cooling from the melt, nor does it cold-crystallize readily upon heating from the glass. The molecular weight of PETG was estimated from the measured intrinsic viscosity using Mark−Houwink parameters for PET as described previously.[30] Polystyrene was supplied by The Dow Chemical Co. (Styron 685D). A series of styrene−acrylonitrile copolymers (SAN) were obtained: SAN17 was provided by Bayer Polymers (Lustran SAN Sparkle); SAN25 and SAN30 were supplied by The Dow Chemical Co. (Tyril 100 and Tyril 880, respectively). The number following the SAN abbreviation represents the weight percent acrylonitrile in the copolymer as given by the manufacturer and confirmed by infrared spectroscopy.[31] The styrenic resins were received in the form of pellets and used without further purification. Molecular weights of PS and SAN copolymers were determined using GPC. The instrument was calibrated with polystyrene standards. The M_w and polydispersity index PDI $= M_w/M_n$ are given in Table 1.

Films with microlayer and nanolayer architectures were fabricated using the layer-multiplication process illustrated in Figure 2. The extruder temperatures were adjusted to ensure that the viscosities matched when the melts were combined in the feed block. Metering pumps ensured that the feed ratio was 1:1 (v:v). The assembly of die elements was always maintained at 240 °C so that the interphase would form at the same temperature in all cases. After the melt exited the assembly of n die elements with $2^{(n+1)}$ layers, it was spread in a film die to further reduce the layer thickness. Rapid quenching on a chill roll equipped with an air knife froze the melt morphology. Films composed of alternating layers of PETG and either PS or SAN were processed into 32 layers (4 die elements), 512 layers (8 die elements), and 4096 layers (11 die elements) with total film thicknesses ranging from 400 to 20 μm. The nominal layer thickness d_0 was taken as the film thickness divided by the number of layers and ranged from more than 10 μm to a few nanometers. The thinnest layers were less than the end-to-end distance of the polymer molecules (∼20−50 nm).

For atomic force microscopy (AFM), a film was embedded in 5 min epoxy and cured overnight at 23 °C. Cured specimens were sectioned perpendicular to the plane of the film with an Ultramicrotome (MT6000-XL from RMC, Tucson, AZ). The surfaces were examined in air at ambient conditions using the tapping mode of the Nanoscope IIIa MultiMode scanning probe microscope (Digital Instruments). Phase and height images were recorded simultaneously. Phase images most clearly revealed the layer structure. To resolve the layer structure at the nanoscale, measurements were performed using Si probes with a spring constant of 50 N m^{-1} and resonance frequency in the 284−362 kHz range. The probe radius was 5−10 nm.

The glass transition temperature T_g of the constituent polymers was determined by differential scanning calorimetry. Thermograms were obtained with a Perkin-Elmer DSC-7 using a heating rate of 10 °C min^{-1} over the temperature range from 30 to 160 °C.

The density was measured with a density gradient column constructed from an aqueous solution of calcium nitrate in accordance with ASTM-D 1505 method B. The column was calibrated with glass floats of known density. Small pieces of film (∼25 mm^2) were placed in the column and allowed to equilibrate for 30 min before the measurements were taken. The standard deviation was within ±0.0005 g cm^{-3} for four specimens.

Positron annihilation lifetime spectroscopy (PALS) was performed at 23 °C using a conventional fast−fast coincidence system. The instrumentation and procedures for data analysis were described previously.[32] Ten spectra were collected for each specimen, and the standard deviation of resulting mean free volume hole radius was within ±0.01 Å.

The oxygen flux $J(t)$ at 0% relative humidity, pressure p of 1 atm, and 23 °C was measured with a MOCON OX-TRAN 2/20. The instrument was calibrated using NIST certified Mylar films of known transport characteristics. To obtain accurate permeability $P = Jl/p$, the average thickness l of each specimen was determined as $l = W(A\rho)^{-1}$, where W is the specimen weight, A is the specimen area, and ρ is the density. The error in determining permeability was estimated not to exceed 3%.

Delamination strength was measured at 23 °C with the T-peel test (ASTM D 1876) using 400 μm thick specimens of 1:1 (v:v) composition with 32 layers and nominal layer thickness of 12.5 μm. To initiate crack propagation, specimens 10 mm wide were notched at the center. Peel tests were conducted with a 500 g load cell in a universal testing machine (Instron 1123) at a cross-head speed of 10 mm min^{-1}. For each composition, 5−7 specimens were tested. The crack propagated at a relatively constant load P_{cr} from which the delamination strength $G_{IC} = 2P_{cr}/W$ was obtained for a specimen of width W. Decreasing the cross-head speed had almost no effect on G_{IC}. The beam arms returned to their original position upon removal of the load, indicating that the contribution of beam arm deformation to delamination strength was negligible. The peeled surfaces were characterized with a Nicolet 870 Nexus FT-IR spectrometer with a photoacoustic attachment (FTIR-PAS). The penetration depth of the acoustic signal used was in the range of 3−5 μm, which is significantly smaller than individual layer thickness of 12.5 μm. The peeled surfaces were also examined using scanning electron microscopy (SEM) (JEOL 840A) with about 90 Å of gold coating.

Results and Discussion

Oxygen Permeability. All the films studied were characterized by a continuous and uniform layered structure as revealed by the atomic force microscope. As an example, Figure 3 shows phase images of PETG/PS films with 60, 30, and 8 nm layers. In each image, the PETG layers are smooth and bright whereas the PS layers are dark and somewhat hackled due to brittle fracture during microtoming. Well-resolved PETG and PS layers are observed in films with 60 and 30 nm layers (Figure 3a,b). Imaging films with the thinnest layers requires exceptionally high-quality microtomed surfaces. Nevertheless, layering is clearly discernible in regions of the film with 8 nm layers (Figure 3c). In all cases, the average layer thickness measured from phase images corresponds well with the nominal layer thickness d_0. Therefore, layer thickness is given as d_0 in subsequent discussions.

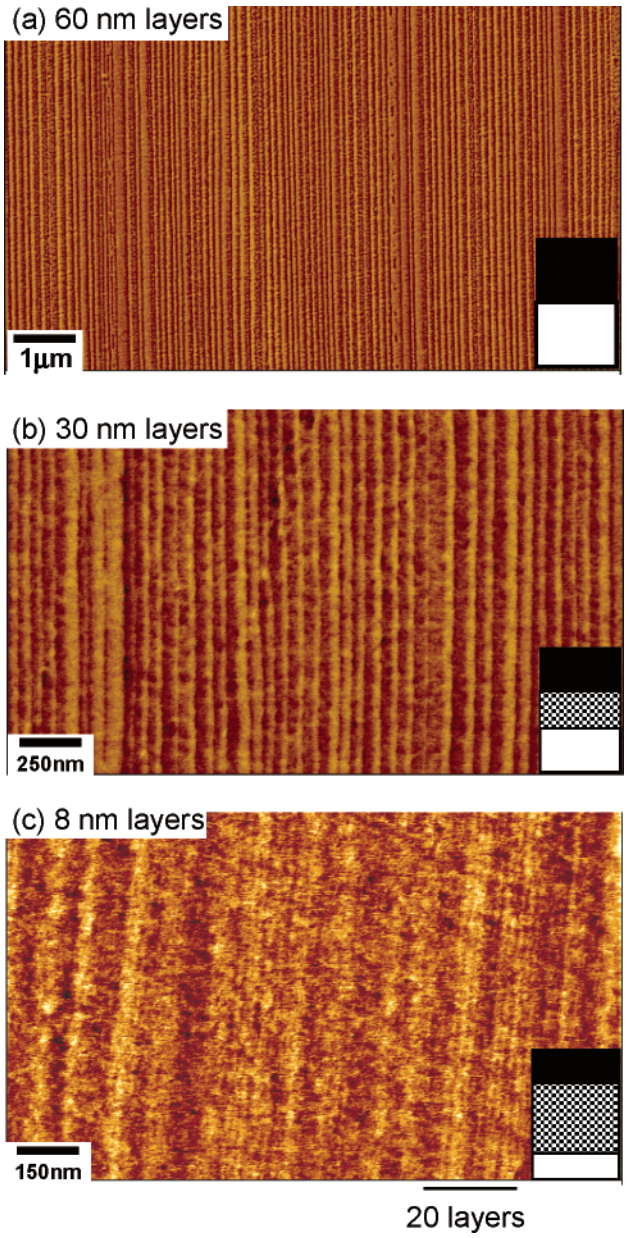

Figure 3. AFM phase images showing cross-sections of PETG/PS assemblies with different layer thicknesses.

The oxygen permeability P of PETG/SAN25 is plotted as a function of layer thickness d_0 in Figure 4a. For d_0 thicker than ~100 nm, P is essentially independent of layer thickness. The series model for permeability of a laminated A−B composite structure of 1:1 (v:v) composition is

$$P_d = 2\left[\frac{1}{P_A^o} + \frac{1}{P_B^o}\right]^{-1} \quad (5)$$

where P_A^o and P_B^o are the permeabilities of A and B, respectively. The value of P_d calculated for PETG/SAN25 is represented by the lower dashed line in Figure 4a. The measured P of about 1.23 cm^3 (STP) cm m^{-2} day^{-1} atm^{-1} for films with layers thicker than 100 nm corresponds to P_d. Thus, the film can be described as an array of discrete layers that exhibits the constituent properties. However, as the layer thickness decreases below 100 nm, P increases rapidly until the layer thickness is in the range of 10 nm. Decreasing

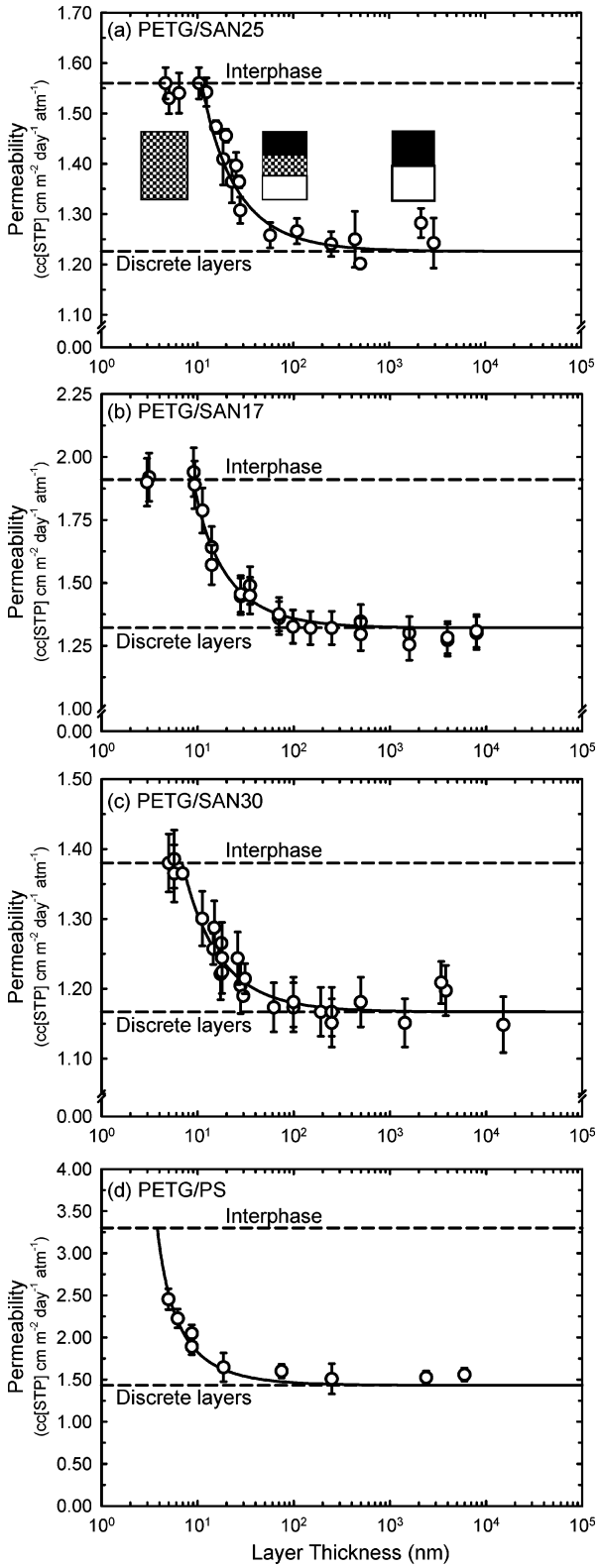

Figure 4. Effect of layer thickness on oxygen permeability of PETG/SAN assemblies: (a) PETG/SAN25, (b) PETG/SAN17, (c) PETG/SAN30, and (d) PETG/PS. The solid lines indicate the best fit of the data to eq 7; the upper and lower dashed lines indicate P_I and P_d, respectively.

the layer thickness further does not affect P. The maximum P of 1.56 cm^3 (STP) cm m^{-2} day^{-1} atm^{-1} is taken as the interphase permeability P_I and is represented by the upper dashed line in Figure 4a This value is fairly close to the permeability of a homogeneous

1:1 (v:v) mixture P_h given as[5]

$$\ln P_h = \phi_A \ln P_A^o + \phi_B \ln P_B^o \qquad (6)$$

For PETG/SAN25, the calculated P_h is 1.59 cm^3 (STP) cm m^{-2} day^{-1} atm^{-1}.

To describe the dependence of gas permeability for films with layer thickness $d_0 \leq 100$ nm and to obtain the interphase thickness d_I, films with $d_0 \geq d_I$ are assumed to possess symmetrical interphases of constant thickness d_I. The dependence of P on layer thickness is then given by a three-layer composite model, in which constituent layers of thickness $(d_0 - d_I)$ are sandwiched between interphase layers of thickness $d_I/2$:

$$P = 2\left[\frac{d_0 - d_I}{d_0}\left(\frac{1}{P_A^o} + \frac{1}{P_B^o}\right) + 2\frac{d_I}{d_0}\left(\frac{1}{P_I}\right)\right]^{-1} \qquad (7)$$

Equation 7 is formulated for films with a 1:1 (v:v) composition only. The first term of eq 7 is the contribution of constituent layers. The second term is the interphase contribution and dominates as d_0 approaches d_I. When the layers are thin enough that $d_0 < d_I$, the film is totally interphase with permeability $P = P_I$. Taking P_I of 1.56 cm^3 (STP) cm m^{-2} day^{-1} atm^{-1} for the PETG/SAN25 interphase, the data for $d_0 \geq d_I$ are fit to eq 7 with the interphase thickness d_I as the only adjustable parameter. The best fit as represented by the solid line in Figure 4a is obtained with $d_I = 11$ nm. The fit is sensitive enough to give d_I to two significant figures.

Because thickness variation on the order of 20% is inherent to all the microlayer and nanolayer films, it is important to determine whether this variation is acceptable for obtaining a reliable value of d_I. For this purpose, the permeability P of a film with periodic layer thickness variation is modeled. The layer thickness variation is considered to have the form $d = d_0[1 + \delta_0 \sin(z/\lambda)]$, where d_0 is the nominal layer thickness, δ_0 is the relative amplitude of the variation, z is the length scale through the film, and λ is the corresponding period. If $\lambda \gg d_0$, the permeability can be calculated from eq 7 with $d = d(z)$ and then averaged over the period λ. The results are shown in Figure 5 for several values of δ_0. Deviation Δ from the uniform layer assumption is included in the insets. Layer thickness variation has no effect on P unless $d_0 < d_I + \delta_0$. Then, the effect is to decrease P and blunt the P vs d_0 relationship as d_0 approaches d_I. For $\delta_0 = 0.1$, which corresponds to a minimum to maximum layer thickness variation of 20%, the maximum deviation in P is less than 5%, which is comparable to the experimental uncertainty in the measurement of P. The effect of layer thickness variation is more perceptible with larger δ_0. However, even for $\delta_0 = 0.2$, which corresponds to a layer thickness variation of 40%, only a small part of the permeability curve is affected. The unaffected region encompasses a large enough change in P that d_I can be reliably obtained by fitting eq 7 to the experimental measurements for larger d_0.

Oxygen permeability of PETG/SAN17 and PETG/SAN30 films also increases as the layer thickness approaches the nanoscale (Figure 4b,c). Films with layers thicker than 100 nm possess constant permeability of about 1.32 cm^3 (STP) cm m^{-2} day^{-1} atm^{-1} for PETG/SAN17 and 1.17 cm^3 (STP) cm m^{-2} day^{-1} atm^{-1} for PETG/SAN30. These values conform to P_d calculated from eq 5, and they are indicated by the lower dashed line in each of the figures. As d_0 decreases from 100 nm to about 10 nm, P rapidly increases to 1.91 cm^3 (STP) cm m^{-2} day^{-1} atm^{-1} for PETG/SAN17 and 1.38 cm^3 (STP) cm m^{-2} day^{-1} atm^{-1} for PETG/SAN30. These values are close to P_h for the homogeneous mixture (Table 2). They are taken as P_I for PETG/SAN17 and PETG/SAN30, respectively, as indicated by the upper dashed lines in Figure 4b,c. The fit to eq 7 yields d_I values of 8.9 nm for PETG/SAN17 and 6.9 nm for PETG/SAN30 (Table 2). The difference in permeability of the constituent polymers is smallest for PETG/SAN30, which accounts for the relatively large scatter in data for this polymer pair.

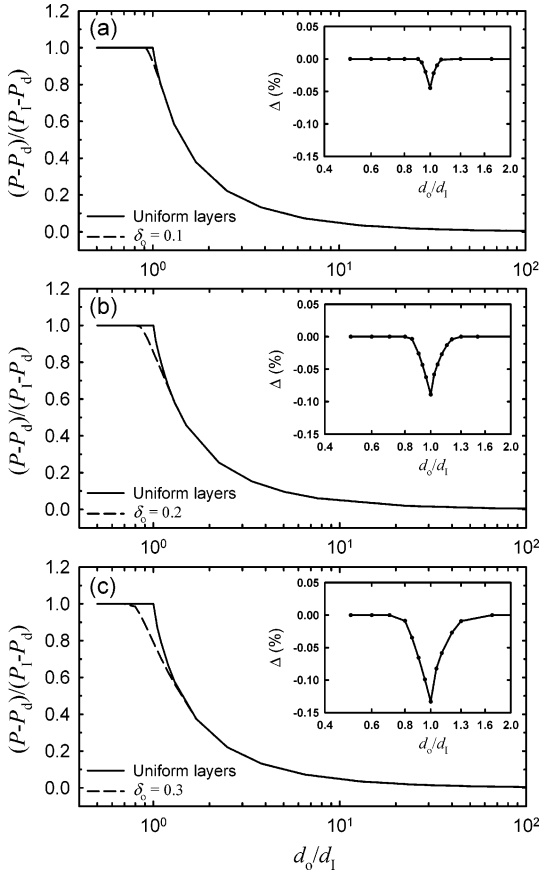

Figure 5. Simulation of the effect of layer thickness variation on permeability based on the three-layer interphase model: (a) $\delta_0 = 0.1$, (b) $\delta_0 = 0.2$, and (c) $\delta_0 = 0.3$. The insets show the deviation Δ from the uniform layer assumption.

Oxygen permeability of PETG/PS is plotted as a function of d_0 in Figure 4d. The value of about 1.43 cm^3 (STP) cm m^{-2} day^{-1} atm^{-1} for films with thicker layers conforms to eq 5 and is taken as P_d for this polymer pair. As d_0 decreases below about 100 nm, P increases continuously without reaching a constant value. The highest permeability measured for a PETG/PS film is 2.45 cm^3 (STP) cm m^{-2} day^{-1} atm^{-1} for a film with 4096 layers, film thickness of 20.3 μm, and d_0 of about 5 nm. Despite the large increase in P compared to P_d, P of the film with 5 nm layers is significantly smaller than P_h from eq 6 of 3.30 cm^3 (STP) cm m^{-2} day^{-1} atm^{-1}. In this case, the interphase thickness is less than 5 nm, and a film totally comprised of interphase is not obtained. Assuming that P_h is a good approximation of P_I, eq 7 gives the interphase thickness of PTEG/PS as 3.8 nm.

Interphase Thickness. The experimental result for d_I can be compared with the theoretical prediction as

Table 2. Interphse Properties of Polymer Assemblies[a]

material	χ (10^{-3})	d_I (nm)	P_d	P_h	P_I	ρ_d (g cm^{-3})	ρ_I (g cm^{-3})	r_d (Å)	r_I (Å)	G_{IC} (J m^{-2})
PETG/PS	47.1	3.8	1.43	3.30		1.1624	1.1677[b]	2.71	2.63[b]	15 ± 5
SAN17	2.9	8.9	1.32	2.03	1.91	1.1732	1.1790	2.64	2.55	61 ± 10
SAN25	2.4	11	1.23	1.59	1.56	1.1796	1.1805	2.63	2.59	70 ± 10
SAN30	7.3	6.9	1.17	1.40	1.38	1.1815	1.1902	2.63	2.50	41 ± 6

[a] χ, interaction parameter; d_I, interphase thickness; P_d, permeability of discrete layers from eq 5 in cm^3 (STP) cm m^{-2} day^{-1} atm^{-1}; P_h, permeability of homogeneous mixture from eq 6 in cm^3 (STP) cm m^{-2} day^{-1} atm^{-1}; P_I, permeability of interphase in cm m^{-2} day^{-1} atm^{-1}; ρ_d, density of discrete layers; ρ_I, density of interphase; r_d, free volume hole radius of discrete layers; r_I, free volume hole radius of interphase; G_{IC}, interphase strength. [b] Estimated, see text.

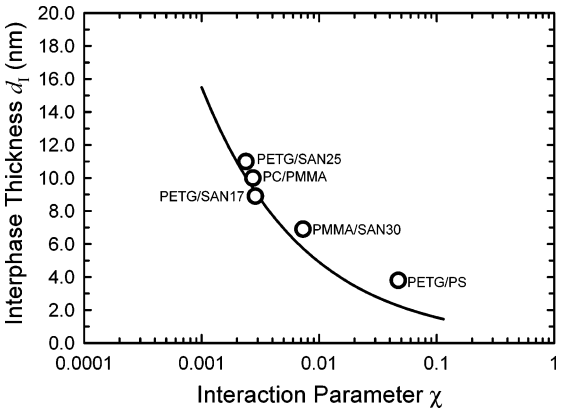

Figure 6. Relationship between interphase thickness and interaction strength as expressed by the χ parameter. The line represents the prediction given by eq 4. Data for PC/PMMA from ref 25.

expressed in eq 4 if the interaction parameter χ is known. The interaction parameter χ_{AB} for the A/B polymer pair is obtained from the solubility parameters of the constituents δ_A and δ_B according to the expression

$$\chi_{AB} = \frac{V}{RT}(\delta_A - \delta_B)^2 \qquad (8)$$

where V is the reference molar volume taken as the average for polymers A and B, and T is taken as the processing temperature of 513 K. Typically, χ is a small number, and therefore it is very sensitive to the choice of δ_A and δ_B. However, for any given polymer, a large range of δ values is often reported due to the relatively large method-to-method variation.[33] To minimize such effects, solubility parameters of PS and SAN copolymers are taken from the linear relationship between δ and acrylonitrile content constructed with data from a single source.[34] The values of δ given in Table 1 are for ambient temperature. However, assuming that the temperature dependence of δ is about the same for all the polymers studied, the quantity $(\delta_A - \delta_B)$ is essentially temperature independent. Indeed, the assumption that $(\delta_A - \delta_B)$ can be taken as a constant in eq 8 is supported by the experimental observation that χ varies as T^{-1}.[35,36]

For PETG, δ is not known and is incorporated into the analysis as a fitting parameter. As expected, χ is very sensitive to the value of δ chosen for PETG. A value of 19.70 J$^{0.5}$ cm$^{-1.5}$ gives the results in Figure 6, where d_I from permeability is compared with the prediction from eq 4 as represented by the solid line. Included in the plot is the interphase thickness reported previously for PC/PMMA nanolayers.[25] Experimental results for polymer pairs with thicker interphases, i.e., PETG/SAN17, PETG/SAN25, and PC/PMMA, show excellent agreement. For polymer pairs with relatively thin interphases, PETG/PS and PETG/SAN30, the experimental results are slightly higher than the prediction. The small discrepancy may originate from the infinite molecular weight assumption of the theory, as compared to the polydispersity of "real" polymers.

The composition dependence of χ exhibits a shallow minimum near PETG/SAN25. Following the approach used to describe a similar minimum in χ of PC/SAN,[37] the data are described by the empirical expression

$$\chi = T^{-1}(164\phi_{AN}^2 - 104\phi_{AN} + 48.0) \qquad (9)$$

where T is the process temperature of 513 K and ϕ_{AN} is the mole fraction acrylonitrile in the copolymer. Equation 9 gives a broad minimum in χ at ϕ_{AN} of 0.32.

Interphase Strength. The strength of the interphase depends on physical entanglement of chains crossing the interface. A minimum of one entanglement is required for good stress transfer,[38] and at least eight may be required for maximum strength.[39−41] The number of entanglements can be estimated by comparing the thickness of the interphase with the radius of gyration $R_{g,e}$ of the entanglement molecular weight M_e. Assuming that PETG has roughly the same molecular dimensions as polycarbonate, $R_{g,e} = 0.457\sqrt{M_e}$ with $M_e = 1500$ g mol^{-1}.[42] Similarly, assuming SAN copolymers have roughly the same molecular dimensions as PS, $R_{g,e} = 0.275\sqrt{M_e}$ with $M_e = 13\,000$ g mol^{-1}.[42] The number of entanglements across the interphase, estimated as $d_I/\langle R_{g,e}\rangle$, where $\langle R_{g,e}\rangle$ is the average of the constituents, is on the order of only 2−5.

The interphase strength is measured by the standard T-peel method using relatively thick microlayers in order to confine fracture to a single interphase.[16,17] Examination of peeled specimens in the optical microscope confirms that the crack propagates along a single interphase. In the SEM, the peeled surfaces are featureless with no evidence of crazing, which would be visible at the 10 μm size scale.[43] If a significant amount of one polymer is ripped off during fracture, a surface technique such as photoacoustic FTIR is sensitive enough to detect the residue. However, virtually clean spectra are obtained for all the fracture surfaces. The combined observations from microscopy and FTIR indicate that the crack propagates through the interphase, and therefore the T-peel test measures the interfacial strength. The results of T-peel tests are summarized in Table 2. Interfacial strength G_{IC} ranges from 15 ± 5 J m^{-2} for PETG/PS to 70 ± 10 J m^{-2} for PETG/SAN25. The values are comparable to those reported previously for interfacial failure of PC/SAN microlayers.[16] According to the minor chain diffusion model, $G_{IC} \propto d_I^2$.[40] From the plot of G_{IC} at 23 °C vs d_I in Figure 7, it appears that the interfacial strength of PETG/SAN conforms to the predicted squared dependence on d_I. However, the data scatter enough that a linear relationship is also possible.

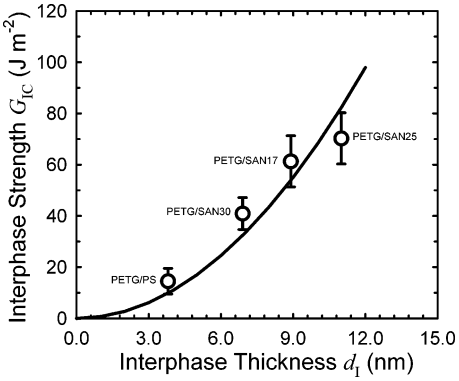

Figure 7. Relationship between interfacial strength and interphase thickness. The solid line represents the squared relationship.

Interphase Free Volume. The density ρ_d of microlayer films that have negligible interphase is compared with the density ρ_I of nanolayer films that are totally interphase in Table 2. The density of microlayers approximately conforms to the additive value $\rho_d = \rho_A\phi_A + \rho_B\phi_B$ based on the constituent densities. The interphase density ρ_I of nanolayers is consistently higher than ρ_d. The largest increase in density of 0.0087 g cm^{-3} occurs with PETG/SAN30, whereas the smallest increase of 0.0009 g cm^{-3} occurs with PETG/SAN25. Although the density change is relatively small, it is significantly higher than the uncertainty in the density measurements of ±0.0005 g cm^{-3}. The higher density of interphase materials suggests a loss in free volume compared to the constituents.

Positron annihilation lifetime spectroscopy is a powerful probe of free volume structure at the molecular scale.[44−47] Examination of free volume hole radius r for the constituent polymers reveals a large difference between PETG, 2.52 Å, and the styrenic polymers, 2.72−2.85 Å (Table 1). The fractional free volume FFV can be calculated according to

$$\mathrm{FFV} = (4\pi/3)r^3N_0 \tag{10}$$

where N_0 is the hole density. Various PALS studies, considering either an average hole size[47−49] or a distribution of hole sizes,[50] yield a free volume hole density N_0 of about 4.0×10^{20} cm^{-3} at 23 °C for a wide range of polymers. This value of N_0 is used to calculate FFV values given in Table 1. Because of the smaller hole size, PETG has lower FFV (0.027) than PS and SAN copolymers (0.034−0.039). According to free volume concepts that relate the amount of excess-hole free volume in the nonequilibrium glass to the temperature difference from T_g,[26] lower free volume of PETG is consistent with its lower T_g (82 °C) compared to those of PS and SAN (102−108 °C).

Microlayer films with discrete layers possess mean hole radii r_d that are close to the additive values based on the constituents (Table 2). The higher density of nanolayers corresponds with a smaller hole radius r_I as determined by PALS (Table 2). The hole radius decreases the most for PETG/SAN30, by 0.13 Å from 2.63 Å to 2.50 Å. This polymer pair also shows the largest increase in density. Similarly, the hole radius decreases the least for PETG/SAN25, by 0.04 Å from 2.63 Å to 2.59 Å, which is consistent with the smallest density increase observed with this pair.

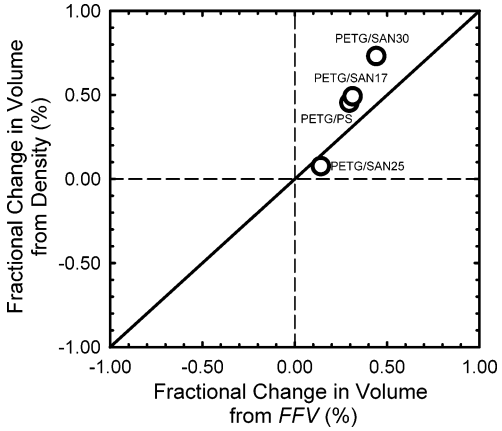

Figure 8. Deviation in interphase volume from the additive prediction based on constituent properties. The result from density is compared to the result from free volume.

Assuming that the occupied volume is unchanged by interfacial mixing and higher density of the interphase is solely due to decreased free volume, the fractional change in volume ($\Delta V/V$) from density, given as

$$\frac{\Delta V}{V} = \frac{\nu_d - \nu_I}{\nu_d} \tag{11}$$

where $\nu = \rho^{-1}$ is the specific volume and the subscripts refer to discrete layers and interphase, is compared with fractional change in volume from FFV given as

$$\frac{\Delta V}{V} = \frac{\mathrm{FFV_d} - \mathrm{FFV_I}}{1 - \mathrm{FFV_I}} \tag{12}$$

where fractional free volumes of discrete layers $\mathrm{FFV_d}$ and interphase $\mathrm{FFV_I}$ are calculated from r_d and r_I, respectively, using eq 10 and assuming constant hole density N_0 of 4.0×10^{20} cm^{-3} at 23 °C.

For PETG/SAN17, PETG/SAN25, and PETG/SAN30, films with the thinnest layers are completely interphase. Therefore, the interphase density and free volume hole size are directly measured. However, in the case of the PETG/PS, a completely interphase film is not obtained. An additive model is used to estimate the interphase properties from measurements on film with nanolayers 5.0 nm thick and interphase volume fraction of 76%. All the values are reported in Table 2. The fractional change in volume from density (eq 11) is compared with that from FFV (eq 12) in Figure 8. Reasonably good agreement suggests that a change in molecular scale free volume hole size is responsible for the observed change in density.

It is surprising that the PETG/SAN30 interphase undergoes the largest volume change, whereas PETG/SAN25 undergoes the least. The changes for PETG/SAN17 and PETG/PS are intermediate. Clearly, the volumetric change does not directly correlate with χ. Both positive and negative deviations in free volume additivity reported in blends of more compatible polymers also have no direct correlation with χ.[51] It is postulated that segmental conformation and packing rather than specific interactions are responsible for the changes. However, no quantitative formulation has been proposed, and the origin of nonadditive volume changes upon interfacial mixing of compatible polymers remain an open question. This subject is addressed in ongoing investigations of nanolayer assemblies where interac-

tion strength, molecular weight, and entanglement molecular weight are systematically varied.

Conclusions

Forced assembly of immiscible polymers into layered nanostructures by layer-multiplying coextrusion makes it possible to probe the interphase with conventional tools of polymer analysis. Continuous, uniform layers in coextruded assemblies of a copolyester (PETG) and a compatible styrenic polymer (PS or SAN) are revealed in AFM phase images. When individual layers are much thicker than the interfacial dimension, properties of the assembly follow series predictions based on the constituent properties. As the layer thickness approaches the dimension of the polymer molecule (20−50 nm), the effects of interfacial molecular mixing are detected. Further reduction in layer thickness to the dimension of the interphase creates a new material that is entirely interphase. The interphase thickness, as determined from the layer thickness dependence of oxygen permeability, and interphase strength, as determined by the T-peel test, depend on interaction strength in accordance with model predictions based on the χ parameter. Unexpectedly, volumetric properties of the interphase exhibit small but significant deviations from the additive predictions. Correspondence between the decrease in specific volume from macroscopic density measurements and the decrease in free volume hole size from PALS suggests that densification of the interphase occurs primarily by a decrease in free volume hole size rather than by a decrease in the number of free volume holes. The volume change does not directly correlate with interaction strength as represented by the χ parameter. At present, the origin of the volume change is not clear and is the subject of ongoing investigation.

Acknowledgment. This research was generously supported by NSF (Grant DMR-0349436) and DARPA (Grant MDA972-02-1-0011). Support from Modern Controls, Inc., for development of a facility for gas-transport studies at Case Western Reserve University is gratefully acknowledged.

References and Notes

(1) Jérôme, B.; Commandeur, J. *Nature (London)* **1997**, *386*, 589−592.
(2) Zheng, X.; Sauer, B. B.; Vanalsten, J. G.; Schwarz, S. A.; Rafailovich, M. H.; Sokolov, J.; Rubinstein, M. *Phys. Rev. Lett.* **1995**, *74*, 407−410.
(3) Forrest, J. A.; Dalnoki-veress, K. *J. Polym. Sci., Part B: Polym. Phys.* **2001**, *39*, 2664−2670.
(4) Sharma, A.; Reiter, G. *J. Colloid Interface Sci.* **1996**, *178*, 383−399.
(5) Paul, D. R., Bucknall, C. B., Eds. *Polymer Blends*; Wiley: New York, 2000; Vols. 1 and 2.
(6) Helfand, E.; Tagami, Y. *J. Polym. Sci., Polym. Lett.* **1971**, *9*, 741−746.
(7) Helfand, E.; Tagami, Y. *J. Chem. Phys.* **1972**, *56*, 3592−3601.
(8) Helfand, E.; Sapse, A. M. *J. Chem. Phys.* **1975**, *62*, 1327−1331.
(9) Helfand, E. *J. Chem. Phys.* **1975**, *63*, 2192−2198.
(10) Utracki, L. A. *Polymer Alloys and Blends: Thermodynamics and Rheology*; Hanser Publishers: Munich, 1990; pp 118−124.
(11) Merfeld, G. D.; Paul, D. R. In *Polymer Blends*; Paul, D. R., Bucknall, C. B., Eds.; Wiley: New York, 2000; Vol. 1, p 55 ff.
(12) Farinha, J. P. S.; Vorobyova, O.; Winnik, M. A. *Macromolecules* **2000**, *33*, 5863−5873.
(13) Baer, E.; Hiltner, A.; Keith, H. D. *Science* **1987**, *235*, 1015−1022.
(14) Kerns, J.; Hsieh, A.; Hiltner, A.; Baer, E. *J. Appl. Polym. Sci.* **2000**, *77*, 1545−1557.
(15) Kerns, J.; Hsieh, A.; Hiltner, A.; Baer, E. *Macromol. Symp.* **1999**, *147*, 15−25.
(16) Ebeling, T.; Hiltner, A.; Baer, E. *J. Appl. Polym. Sci.* **1998**, *68*, 793−805.
(17) Ebeling, T.; Hiltner, A.; Baer, E. *Polymer* **1999**, *40*, 1525−1536.
(18) Ebeling, T.; Hiltner, A.; Baer, E. *Polymer* **1999**, *40*, 1985−1992.
(19) Ronesi, V.; Cheung, Y. W.; Hiltner, A.; Baer, E. *J. Appl. Polym. Sci.* **2003**, *89*, 153−162.
(20) Poon, B. C.; Chum, S. P.; Hiltner, A.; Baer, E. *J. Appl. Polym. Sci.* **2004**, *92*, 109−115.
(21) Poon, B. C.; Chum, S. P.; Hiltner, A.; Baer, E. *Polymer* **2004**, *45*, 893−903.
(22) Pollock, G.; Nazarenko, S.; Hiltner, A.; Baer, E. *J. Appl. Polym. Sci.* **1994**, *52*, 163−176.
(23) Mueller, C. D.; Nazarenko, S.; Ebeling, T.; Schuman, T. L.; Hiltner, A.; Baer, E. *Polym. Eng. Sci.* **1997**, *37*, 355−362.
(24) Schuman, T.; Stepanov, E. V.; Nazarenko, S.; Capaccio, G.; Hiltner, A.; Baer, E. *Macromolecules* **1998**, *31*, 4551−4561.
(25) Liu, R. Y. F.; Jin, Y.; Hiltner, A.; Baer, E. *Macromol. Rapid Commun.* **2003**, *24*, 943−948.
(26) Polyakova, A.; Liu, R. Y. F.; Schiraldi, D. A.; Hiltner, A.; Baer, E. *J. Polym. Sci., Part B: Polym. Phys.* **2001**, *39*, 1889−1899.
(27) Liu, R. Y. F.; Schiraldi, D. A.; Hiltner, A.; Baer, E. *J. Polym. Sci., Part B: Polym. Phys.* **2002**, *40*, 862−877.
(28) Hu, Y. S.; Liu, R. Y. F.; Zhang, L. Q.; Rogunova, M.; Schiraldi, D. A.; Nazarenko, S.; Hiltner, A.; Baer, E. *Macromolecules* **2002**, *35*, 7326−7337.
(29) Liu, R. Y. F.; Hiltner, A.; Baer, E. *J. Polym. Sci., Part B: Polym. Phys.* **2004**, *42*, 493−504.
(30) Hu, Y. S.; Liu, R. Y. F.; Schiraldi, D. A.; Hiltner, A.; Baer, E. *Macromolecules* **2004**, *37*, 2136−2143.
(31) Scheddel, R. T. *Anal. Chem.* **1958**, *30*, 1303−1303.
(32) Higuchi, H.; Yu, Z.; Jamieson, A. M.; Simha, R.; McGervey, J. D. *J. Polym. Sci., Part B: Polym. Phys.* **1995**, *33*, 2295−2305.
(33) Van Krevelen, D. W. *Properties of Polymers*, 3rd ed.; Elsevier: Amsterdam, 1997; Chapter 7, pp 189−225.
(34) Karam, H. J. In *Polymer Compatibility and Incompatibility: Principles and Practices*; Solc, K., Ed.; MMI Press: Chur, 1982; pp 93−106.
(35) Chen, H. Y.; Chum, S. P.; Hiltner, A.; Baer, E. *Macromolecules* **2001**, *34*, 4033−4042.
(36) Stephens, C. H.; Hiltner, A.; Baer, E. *Macromolecules* **2003**, *36*, 2733−2741.
(37) Willett, J. L.; Wool, R. P. *Macromolecules* **1993**, *26*, 5336−5349.
(38) Creton, C.; Kramer, E. J.; Hadziioannou, G. *Macromolecules* **1991**, *24*, 1846−1853.
(39) Oslanec, R.; Brown, H. R. *Macromolecules* **2003**, *36*, 5839−5844.
(40) Wool, R. P. *Polymer Interfaces: Structure and Strength*; Hanser Publishers: Munich, 1995; Chapter 9, pp 336−376.
(41) Sperling, L. H. *Introduction to Physical Polymer Science*; John Wiley & Sons: New York, 2001; Chapter 11, pp 513−514.
(42) Sperling, L. H. *Introduction to Physical Polymer Science*; John Wiley & Sons: New York, 2001; Chapter 5, pp 165−200.
(43) Creton, C.; Kramer, E. J.; Hui, C. Y.; Brown, H. R. *Macromolecules* **1992**, *25*, 3075−3088.
(44) Ruan, M. Y.; Moaddel, H.; Jamieson, A. M.; Simha, R.; McGervey, J. D. *Macromolecules* **1992**, *25*, 2407−2411.
(45) McCullagh, C. M.; Yu, Z.; Jamieson, A. M.; Blackwell, J.; McGervey, J. D. *Macromolecules* **1995**, *28*, 6100−6107.
(46) Higuchi, H.; Jamieson, A. M.; Simha, R. *J. Polym. Sci., Part B: Polym. Phys.* **1996**, *34*, 1423−1426.
(47) Srithawatpong, R.; Peng, Z. L.; Olson, B. G.; Jamieson, A. M.; Simha, R.; McGervey, J. D.; Maier, T. R.; Halasa, A. F.; Ishida, H. *J. Polym. Sci., Part B: Polym. Phys.* **1999**, *37*, 2754−2770.
(48) Dlubek, G.; Bondarenko, V.; Pionteck, J.; Supej, M.; Wutzler, A.; Krause-Rehberg, R. *Polymer* **2003**, *44*, 1921−1926.
(49) Bamford, D.; Dlubek, G.; Reiche, A.; Alam, M. A.; Meyer, W.; Galvosas, P.; Rittig, F. *J. Chem. Phys.* **2001**, *115*, 7260−7270.
(50) Hong, X.; Jean, Y. C.; Yang, H. J.; Jordan, S. S.; Koros, W. J. *Macromolecules* **1996**, *29*, 7859−7864.
(51) Wu, S. H. *J. Polym. Sci., Part B: Polym. Phys.* **1987**, *25*, 2511−2529.

MA049233R